LA-UR- 992121

Approved for public release; distribution is unlimited.

Title: A Spatial Discretization for Solving the Transport Equation on Unstructured Grids of Polyhedra

Author(s): Kelly Thompson, X-CI
Marvin L. Adams, Texas A&M University

Submitted to: International Conference on Mathematics and Computation, Reactor Physics and Environmental Analysis in Nuclear Applications, 27-30 September, 1999; Madrid, Spain

A Spatial Discretization for Solving the Transport Equation on Unstructured Grids of Polyhedra

Kelly Thompson
Los Alamos National Laboratory
Applied Theoretical and Computing Physics Division, Code Integration Group
Los Alamos, NM 87545
tel: (505) 667-8747 fax: (505) 665-5553
kellyt@lanl.gov

Marvin L. Adams
Texas A&M University
Department of Nuclear Engineering
College Station, TX 77843-3133
tel: (409) 845-4161 fax: (409) 845-6443
mladams@tamu.edu

Abstract

We extend the family of corner balance spatial discretizations to spatial grids of arbitrary polyhedra. This scheme enforces balance on subcell volumes called *corners*. It produces a lower triangular matrix for sweeping, is algebraically linear, is positive in a source-free absorber, and produces a robust and accurate solution in thick diffusive regions. We briefly derive the method, present some analysis results, and demonstrate performance on several very different test problems.

1 Introduction

Recently there has been significant effort devoted to the development of accurate spatial discretization schemes for particle transport on unstructured three-dimensional grids (McGhee, 1996, Morel, 1996, McGhee, 1997, Wareing, 1996, Miller, 1998). This effort has produced spatial discretization methods for hexahedral, degenerate hexahedral, and tetrahedral grids. Here we report our initial effort toward a "corner balance" (CB) discretization for transport on a more general grid that can contain arbitrary polyhedral cells.

Our starting point is a CB method previously reported for two-dimensional grids of arbitrary polygons (Adams, 1997, Adams, 1998). Our goal is a three-dimensional CB method with the following attractive properties: 1) robust and accurate solution in thick diffusive regions; 2) conservation on subcell (corner) volumes; 3) algebraically linearity, 4) positivity in source-free pure absorbers; 5) formulation that permits sweeping with no matrix inversions; 6) minimal spreading of a beam in a vacuum; and 7) 2nd-order or better truncation error. Some of these desired properties (e.g. numbers 3, 4 and 7) are in conflict; in these cases we have prioritized the properties essentially in the order given. (For example, property #3 takes precedence over property #6.)

2 Development of Discretization

2.1 Balance

We begin with the time-independent one-group discrete ordinates transport equation,

$$\vec{\Omega}_m \cdot \vec{\nabla} \psi_m(\vec{r}) + \sigma_t(\vec{r})\psi_m(\vec{r}) = Q_m(\vec{r}) \equiv \frac{1}{4\pi}(\sigma_t - \sigma_a)\phi(\vec{r}) + \frac{1}{4\pi} S(\vec{r}) \,. \tag{1}$$

As with all CB methods, our discretization will preserve balance on *corner* subcells and thus on cells. There is *corner* volume associated with each vertex of each cell as shown in Fig. 1. The cell midpoint, a vertex, and the face midpoints for each face containing the vertex of interest define a corner volume. If we integrate Eq. (1) over the corner volume we have the following balance equation

$$\sum_{f \in c} a_{m,f(c)} \psi_{m,f(c)} + V_c \sigma_{tc} \overline{\psi}_{m,c} = V_c Q_{m,c} \,. \tag{2}$$

Here $a_{m,f(c)}$ represents the dot product between outward normal of each face and the quadrature direction ($\vec{A}_f \cdot \vec{\Omega}_m$).

2.2 Wedges

It is difficult to construct accurate closures for polyhedral cells or corners. To avoid this complication we introduce another subcell volume that we call a *wedge*. A wedge is always a tetrahedron and is defined by a cell vertex, a cell midpoint, a cell-face midpoint, and an edge midpoint. This regularity makes wedges much simpler than corners to work with. Examples of wedges are shown in Fig. 1.

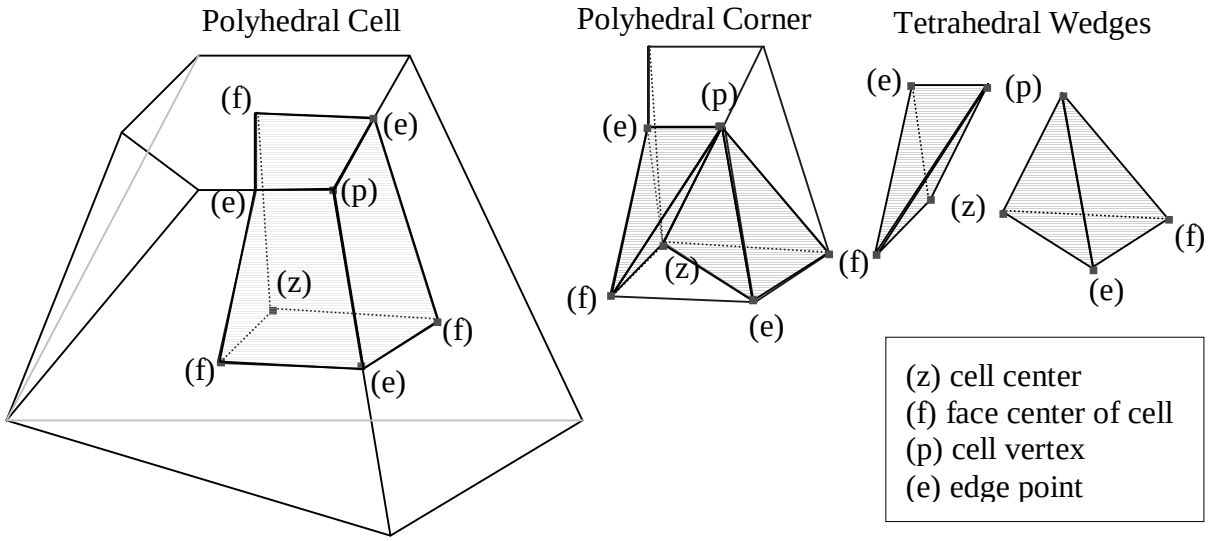

Figure 1. Examples of a cell, a *corner* subcell, and two *wedge* subcells.

We do not enforce particle balance on wedges, but we do enforce the following "pseudo-balance" equation, in which the *corner*-average source appears:

$$a_{m,fep}\psi_{m,fep} + a_{m,fez}\psi_{m,fez} + a_{m,pez}\psi_{m,pez} + a_{m,fpz}\psi_{m,fpz} + \sigma_{t,c}V_w\overline{\psi}_{m,w} = V_w Q_{m,c} \tag{3}$$

Again $a_{m,xxx}$ represents the dot product of the quadrature direction and the outward normal of each wedge face. Since wedges are always tetrahedrons they have four faces, which we have named by their vertices: *fep*, *fez*, *pez* and *fpz*. Note that the sum of Eqs. (3) for all wedges in a corner yields Eq. (2).

2.3 Closure Equations

Our upstream corner balance (UCB) method is defined by the wedge psuedo-balance equation (3) [which ensures balance on corners and cells] in conjunction with *closure equations* that relate surface-averaged and wedge-averaged intensities. We present these closures now, then explain how they produce many of the desired properties that were listed in the introduction.

We choose a "step" closure on the wedge surface, *fep*, that is on the *cell* surface:

$$\psi_{m,fep} = \begin{cases} \psi^{inc}_{w,fep}, & a_{m,fep} < 0 \\ \overline{\psi}_{m,w}, & a_{m,fep} > 0. \end{cases} \tag{4}$$

On wedge surfaces that are internal to a given corner (*fpz* and *pez*) we use:

$$\psi_{m,pez} = \begin{cases} \psi^{inc}_{m,pez} & a_{m,pez} < 0, \\ \overline{\psi}_{m,w} + \frac{1}{3}\left(\left.\frac{Q_m}{\sigma_t}\right|_e + \left.\frac{Q_m}{\sigma_t}\right|_z - 2\left.\frac{Q_m}{\sigma_t}\right|_c \right) + \dfrac{\overline{\psi}_{m,w} - \psi^{inc}_{m,w}}{\left[1+\tau/3+\tau^2/18\right]_{m,w,pez}}, & a_{m,pez} > 0, \end{cases} \tag{5a}$$

$$\psi_{m,fpz} = \begin{cases} \psi^{inc}_{m,fpz} & a_{m,fpz} < 0, \\ \overline{\psi}_{m,w} + \frac{1}{3}\left(\left.\frac{Q_m}{\sigma_t}\right|_f + \left.\frac{Q_m}{\sigma_t}\right|_z - 2\left.\frac{Q_m}{\sigma_t}\right|_c \right) + \dfrac{\overline{\psi}_{m,w} - \psi^{inc}_{m,w}}{\left[1+\tau/3+\tau^2/18\right]_{m,w,fpz}}, & a_{m,fpz} > 0. \end{cases} \tag{5b}$$

We define optical thicknesses and an averaged incident intensity:

$$\tau_{m,w,xxx} = \frac{\sigma_t V_w}{|a_{m,xxx}|}, \tag{6a}$$

$$\overline{\psi}^{inc}_{m,w} = \frac{\sum_{xxx:\, a_{m,xxx}<0} a_{m,xxx}\psi^{inc}_{m,xxx}}{\sum_{xxx:\, a_{m,xxx}<0} a_{m,xxx}}, \tag{6b}$$

for *xxx* = *fep*, *fpz*, *pez*, *fez*. (We shall define the *f*, *e*, and *z* Q/σ_t terms shortly.) Our final closure is on the wedge surface, *fez*, that separates two corners in the same cell:

$$\psi_{m,fez} = \psi^{inc}_{m,fez}, \qquad a_{m,fez} < 0, \tag{7a}$$

$$\begin{aligned} \psi_{m,fez} = \underbrace{\overline{\psi}_{m,w} + \tfrac{1}{2}\left(\left.\frac{Q_m}{\sigma_t}\right|_{c'} - \left.\frac{Q_m}{\sigma_t}\right|_c \right)}_{\text{term 1}} - \underbrace{\frac{\tau_{fep,m,w}}{1+\tau^2_{fep,m,w}} \frac{1}{3}\left(\left.\frac{Q_m}{\sigma_t}\right|_f + \left.\frac{Q_m}{\sigma_t}\right|_e - 2\left.\frac{Q_m}{\sigma_t}\right|_p \right)}_{\text{term 2}} \\ + \underbrace{\left.\frac{3+4\tau}{2\tau\left(1+\tau+2\tau^2\right)}\right|_{fez,m,w} \left(\overline{\psi}_{m,w} - \psi^{inc}_{m,w}\right)}_{\text{term 3}}, \quad a_{m,fez} > 0. \end{aligned} \tag{7b}$$

One of our stated goals is to be able to "sweep" the grid for a given direction *m* one subcell at a time, without having to invert matrices because subcells are coupled. The above closures accomplish this goal; the only "downstream" information needed in a given wedge is source information, which is taken as given during a sweep. Another goal that we have achieved is algebraic linearity, and another is conservation on subcells.

Our fourth stated goal is positivity in source-free pure absorbers. We can show that in the absence of any Q terms the wedge-averaged intensity and all exiting intensities are non-negative given non-negative incident intensities. Thus, we achieve the "positivity" goal.

Our first stated goal is an accurate and robust solution in thick diffusive regions. The above closure equations are designed such that the leading-order UCB solution in a diffusive region will satisfy Palmer's vertex-centered discretization of the diffusion equation (Palmer, 1995). This discretization, which was designed for arbitrary polyhedra, enforces conservation over "dual cells" centered at vertices, where a dual cell is the union of corner subcells that touch the given vertex:

$$\sum_{f,e,z@p} \vec{A}_{fez} \cdot \vec{J}_{fez} + \phi_p \sum_{c@p} V_c \sigma_{a,c} = \sum_{c@p} V_c S_c \,. \tag{8}$$

Here ϕ_p is the scalar flux at the vertex p, and *fez* denotes the surfaces of the dual cell. The summations are over all indicated objects that touch vertex p. Fig. 2 shows a *fez* surface along with the wedges that share it and the two vertices (p and p') that those wedges touch.

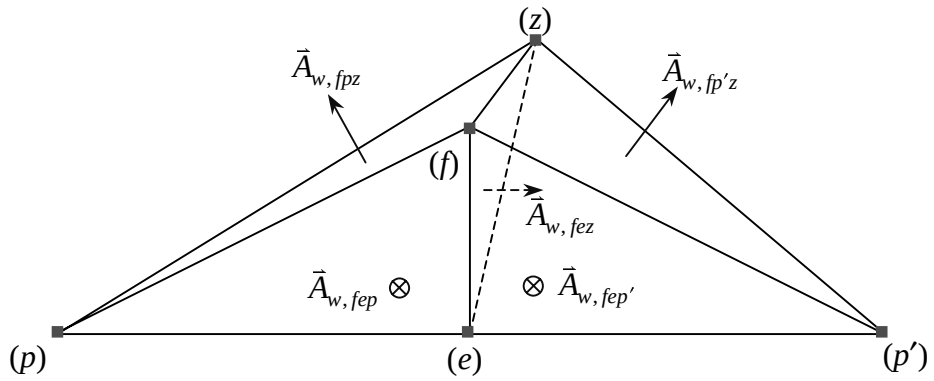

Figure 2. Adjacent wedges in neighboring corners of the same cell.

To complete the definition of Palmer's discretization we must define the net currents across the *fez* surfaces, $\{\vec{J}_{fez}\}$, in terms of the scalar fluxes at vertices, $\{\phi_p\}$. Given cellwise constant cross sections, Palmer's equation for this can be written as follows, where the notation follows Fig. 2.

$$\vec{A}_{fez,w} \cdot \vec{J}_{fez,w} = \frac{-1}{6\sigma_t V_w} \vec{A}_{fez,w} \cdot \begin{bmatrix} \frac{1}{3}\vec{A}_{fep,w}\left(\phi_f + \phi_e + \phi_p\right) + \frac{1}{3}\vec{A}_{fep',w}\left(\phi_f + \phi_e + \phi_{p'}\right) \\ + \frac{1}{3}\vec{A}_{pez,w}\left(\phi_p + \phi_e + \phi_z\right) + \frac{1}{3}\vec{A}_{p'ez,w}\left(\phi_{p'} + \phi_e + \phi_z\right) \\ + \frac{1}{3}\vec{A}_{fpz,w}\left(\phi_f + \phi_p + \phi_z\right) + \frac{1}{3}\vec{A}_{fp'z,w}\left(\phi_f + \phi_{p'} + \phi_z\right) \end{bmatrix} \tag{9}$$

In this equation p' refers to the cell vertex of the wedge that shares the *fez* face with the wedge w, whose cell vertex is p. In Eq. (9) there are scalar fluxes at cell midpoints $\{\phi_z\}$, cell-face midpoints $\{\phi_f\}$, and cell-edge midpoints $\{\phi_e\}$. In Palmer's method each of these is defined to be an interpolant of surrounding vertex scalar fluxes. Eqs. (8), (9), and the interpolating prescriptions (Palmer, 1995) completely define Palmer's diffusion discretization.

We remark that Palmer's interpolations make no error when the exact scalar flux is a linear function of position. Eq. (9) is also exact in that limit; thus, Palmer's scheme exactly captures linear solutions regardless of grid distortion. This is a very strong result and is partly why we chose this method for our wedge-based UCB to mimic in diffusive problems. We further note that the coefficient matrix associated with Palmer's scheme is not symmetric.

We define the *f*, *z*, and *e* Q/σ_t terms in our closure equations to be interpolants of $[Q/\sigma_t]_c$ terms using the Palmer's interpolating formulas. For this purpose, the $[Q/\sigma_t]_c$ for a given corner *c* is treated as if it were the value of Q/σ_t at that corner's vertex *p*. Our method is therefore completely specified by the wedge pseudo-balance equation (2); the closure equations (4), (5), and (7); the definitions (6); and prescriptions for interpolating.

To determine the behavior of our UCB method in thick diffusive regions we employ an asymptotic analysis that has become standard (Adams, 1997). In this analysis we "scale" the cross sections and sources as being O(1) quantities multiplied or divided by a small parameter ε: $\sigma_t \to \sigma_t/\varepsilon$; $\sigma_a \to \varepsilon\sigma_a$; $S \to \varepsilon S$. We expand all unknowns in power series in ε and collect terms of the same ε order in each discrete equation. Brevity requirements prevent a detailed display, but we shall describe some of the key results.

The balance equation (2) causes the leading-order wedge-averaged angular flux to be isotropic and equal for all wedges in a given corner. The closures (4), (5) and (7) cause the leading-order intensities on the *fez*, *fpz*, and *pez* surfaces to be isotropic in thick diffusive regions:

$$\psi^{(0)}_{m,pez} = \frac{1}{4\pi}\frac{1}{3}\left(\phi^{(0)}_c + \phi^{(0)}_e + \phi^{(0)}_z\right), \quad \text{all } m, \tag{10a}$$

$$\psi^{(0)}_{m,fpz} = \frac{1}{4\pi}\frac{1}{3}\left(\phi^{(0)}_c + \phi^{(0)}_f + \phi^{(0)}_z\right), \quad \text{all } m, \tag{10b}$$

$$\psi^{(0)}_{m,fez} = \frac{1}{4\pi}\frac{1}{2}\left(\phi^{(0)}_c + \phi^{(0)}_{c'}\right), \quad \text{all } m, \tag{10c}$$

$$\psi^{(0)}_{m,fep} = \frac{1}{4\pi}\phi^{(0)}_c, \ a_{fep,m} > 0. \tag{10d}$$

Equation (10d) holds for all directions *m* if *fep* is in the interior of the diffusive region; it holds only for outgoing directions if *fep* is on the boundary. In the latter case we find that $\phi^{(0)}_c$ equals a cosine-weighted integral of the incident intensity, which is known as a "Marshak" boundary condition.

A consequence of Eqs. (10a-c) and the *fep* closure (4) is that the leading-order solution is the same in every corner and wedge that touches the same vertex:

$$\overline{\psi}^{(0)}_{m,w} = \overline{\psi}^{(0)}_{m,c} = \frac{1}{4\pi}\phi^{(0)}_c \equiv \frac{1}{4\pi}\phi^{(0)}_p \ \text{ for all wedges } w \text{ and corners } c \text{ touching vertex } p. \tag{11}$$

We now show how Eq. (7b) produces an O(ε) net current that satisfies Eq. (9). First we replace the wedge-averaged unknown in Eq. (7b) using the wedge pseudo-balance equation (2) and solve the resulting equation for $\psi_{m,fez}$:

$$\psi_{m,fez} = \left(\frac{\sigma_t V_w}{\sigma_t V_w + a_{fez,m}}\right)\left\{\begin{array}{c} \frac{1}{2}\left(\frac{Q_m}{\sigma_t}\Big|_{c'} + \frac{Q_m}{\sigma_t}_{c}\right) - \frac{\tau_{fep,m,w}}{1+\tau^2_{fep,m,w}}\frac{1}{3}\left(\frac{Q_m}{\sigma_t}\Big|_f + \frac{Q_m}{\sigma_t}\Big|_e - 2\frac{Q_m}{\sigma_t}\Big|_p\right) \\ -\frac{1}{\sigma_t V_w}\left(a_{fep,m}\psi_{m,fep} + a_{fpz,m}\psi_{m,fpz} + a_{pez,m}\psi_{m,pez}\right) \\ + \frac{3+4\tau}{2\tau\left(1+\tau+2\tau^2\right)}\Big|_{fez,m,w}\left(\overline{\psi}_{m,w} - \psi^{inc}_{m,w}\right) \end{array}\right\}, \quad a_{fez,m} > 0. \tag{12a}$$

The O(ε) component, for $a_{fez,m}>0$, is:

$$\psi^{(1)}_{m,fez} = \tfrac{1}{2}\left(\tfrac{Q_m}{\sigma_t}\Big|_{c'} + \tfrac{Q_m}{\sigma_t}\Big|_{c}\right)^{(1)} - \frac{1}{\tau_{fep,m,w}}\tfrac{1}{3}\left(\tfrac{Q_m}{\sigma_t}\Big|_{f} + \tfrac{Q_m}{\sigma_t}\Big|_{e} - 2\tfrac{Q_m}{\sigma_t}\Big|_{c}\right)^{(0)} - \frac{1}{\tau_{fez,m,w}}\tfrac{1}{2}\left(\tfrac{Q_m}{\sigma_t}\Big|_{c'} + \tfrac{Q_m}{\sigma_t}{}_{c}\right)^{(0)} - \tfrac{1}{\sigma_t V_w}\left(a_{fep,m}\psi_{m,fep} + a_{fpz,m}\psi_{m,fpz} + a_{pez,m}\psi_{m,pez}\right)^{(0)}. \tag{12b}$$

The O(ε) net current across the *fez* surface follows from Eq. (12b) its counterpart for $a_{fez,m}<0$:

$$\begin{aligned}
\vec{A}_{fez,w}\cdot\vec{J}^{(1)}_{m,fez} &= \vec{A}_{fez,w}\cdot\sum_{a_{fez}>0} w_m\vec{\Omega}_m\psi^{(1)}_{m,w,fez} + \vec{A}_{fez,w}\cdot\sum_{a_{fez}<0} w_m\vec{\Omega}_m\psi^{(1)}_{m,w',fez} \\
&= -\tfrac{1}{6\sigma_t V_w}\vec{A}_{fez,w}\cdot\left[\vec{A}_{fep,w}\tfrac{1}{3}\left(\phi_f+\phi_e-2\phi_c\right)^{(0)} + \vec{A}_{fep',w}\tfrac{1}{3}\left(\phi_f+\phi_e-2\phi_{c'}\right)\right] \\
&\quad -\tfrac{1}{6\sigma_t V_w}\vec{A}_{fez,w}\cdot\left[\vec{A}_{fep,w}\phi^{(0)}_c + \vec{A}_{fep',w}\phi^{(0)}_{c'}\right] \\
&\quad -\tfrac{1}{6\sigma_t V_w}\vec{A}_{fez,w}\cdot\left[\vec{A}_{pez,w}\tfrac{1}{3}\left(\phi_c+\phi_e+\phi_z\right)^{(0)} + \vec{A}_{p'ez,w}\tfrac{1}{3}\left(\phi_z+\phi_e+\phi_{c'}\right)^{(0)}\right] \\
&\quad -\tfrac{1}{6\sigma_t V_w}\vec{A}_{fez,w}\cdot\left[\vec{A}_{fpz,w}\tfrac{1}{3}\left(\phi_f+\phi_z+\phi_c\right)^{(0)} + \vec{A}_{fp'z,w}\tfrac{1}{3}\left(\phi_f+\phi_z+\phi_{c'}\right)^{(0)}\right]
\end{aligned} \tag{13}$$

Here we have assumed that our quadrature set correctly integrates the following half range integral:

$$\sum_{a_{fez}>0} w_m\vec{\Omega}_m\vec{\Omega}_m = \sum_{a_{fez}<0} w_m\vec{\Omega}_m\vec{\Omega}_m = \frac{2\pi}{3}. \tag{14}$$

If we combine terms in Eq. (13) and recognize that Eq. (11) identifies leading-order *corner* scalar fluxes as *vertex* scalar fluxes, we obtain Eq. (9). That is, the asymptotic analysis says that the leading-order UCB solution will satisfy Palmer's discretization in thick diffusive regions. However, the analysis also predicts that the leading-order UCB solution will satisfy Marshak boundary conditions in the presence of unresolved boundary layers. In pathological problems these boundary conditions can lead to significant inaccuracies in the solution; thus, the attainment of our first goal is not complete.

Our remaining goals are good truncation error and minimal spreading of a beam in a vacuum. These goals are in conflict with the goals of positivity and algebraic linearity, and we have been unable to achieve them to the degree that we had originally hoped. We will address this matter further in our discussions of numerical results and future work.

2.4 Summary

We have devised a 3D UCB method with the following properties:

- In a thick diffusive problem with a polyhedral-cell grid the leading-order interior solution satisfies the vertex-centered diffusion discretization developed by Palmer for solving diffusion problems on polyhedral-cell grids. This leading-order solution satisfies a Marshak boundary condition.
- It enforces strict particle conservation on corners (and thus on cells).
- It is algebraically linear and is positive in source-free pure absorbers.
- It allows transport sweeps to proceed wedge by wedge in the direction of particle flow, eliminating any downstream coupling of wedge unknowns and thus eliminating any need for matrix inversions.

3 Numerical Results

In this section, we present the results from test problems designed to illustrate the strengths and weakness of our wedge-based UCB spatial discretization. Our first problem is a fine-mesh study on a regular grid, with comparisons against established methods. The second problem is a fully reflected sphere that demonstrates the polyhedral capability as well as the ability to handle arbitrarily oriented reflecting surfaces. In a third problem we demonstrate numerically its performance in the thick diffusion limit. Unfortunately, due to technical difficulties, we are unable to present this result here. However, preliminary results suggest that even on a distorted grid the wedge-based UCB method exactly captures a linear solution in the thick diffusion limit, which is what one would expect from a scheme that limits to Palmer's diffusion discretization.

Our first XYZ problem compares the new UCB method against the diamond differencing (DD) and linear discontinuous (LD) methods for fine and intermediate cells in regular grids. Results from the latter two methods were obtained from DANTSYS. The test problem is a source-free brick, 2x20x20 mean-free paths, with an isotropic incident intensity on the minimum x-face. The removal cross section is half of the total. There are reflective boundary conditions on the top, bottom, left and right faces to simulate a slab problem. Each problem used a S_4 level-symmetric quadrature set. Each method computed the exiting flow rate (EFR) from the maximum x-face and the total absorption rate (AR) for various mesh spacings. The errors listed in Table 1 were generated by assuming that a 128x128x128 3D LD problem obtains the correct solution.

Table 1. Errors in exiting flow rate (EFR) and absorption rate (AR), various methods and grids.

Number of cells	Method					
	DD error		LD error		3D UCB error	
	AR	EFR	AR	EFR	AR	EFR
2x4x4	N/A		N/A		7.947	6.530
4x4x4	6.646	6.839	1.511	0.641	2.469	1.664
8x4x4	1.669	1.719	0.218	0.087	0.665	0.423
16x4x4	0.330	0.431	0.029	0.012	0.172	0.107
32x4x4	0.104	0.108	0.006	0.002	0.044	0.027
64x4x4	0.026	0.029	0.0	0.001	0.012	0.007

There are several points worth noting. First, both LD and DD will obtain the same solution to this problem that their slab-geometry version would obtain (given the same quadrature set). This solution is independent of the number of cells along the *y* and *z* axes (where the solution is constant). The same is *not* true of the wedge-based UCB scheme we have developed here. It does not obtain the slab-geometry UCB solution except in the limit of large cell dimensions in the *y* and *z* dimensions. As one consequence, this means that (for example) the 32x32x32 UCB solution is less accurate than the 32x4x4 solution in this test problem. While our table seems to indicate that 3D UCB has 2nd-order truncation error, theoretical studies and more extensive numerical studies convince us that rigorously it is only 1st-order accurate.

Our second test problem is a fully-reflected spherical k-eigenvalue problem. Our spherical mesh consists of 19 slices of tetrahedral and hexahedral cells, each slice containing 10 layers of 10 cells as shown in Fig. 3. The 2-group cross section data without up-scatter is as follows: σ_t*=[0.70984, 1.5291],* σ_s*=[0.46025, 0.0, 0.14310, 0.93424],* $\nu\sigma_f$*=[3.9254, 10.8123],* χ*=[0.35345, 0.64655]*. When solved with an S_6 level-symmetric quadrature set, our XYZ UCB scheme produces the solution k_∞=2.01180 while the analytic solution is 2.01185.

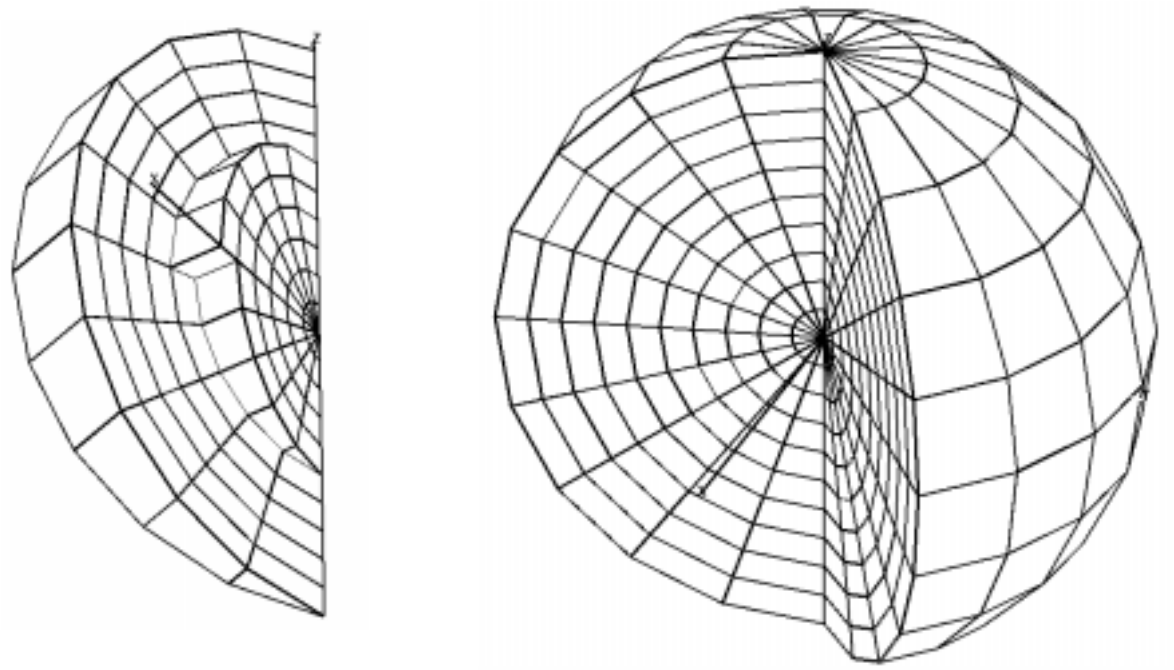

Figure 3. Fully reflected spherical mesh of tetrahedral and hexahedral cells.

We believe that the discrepancy between the analytic and numerical solutions is an artifact of the reflecting boundary algorithm used on the arbitrarily oriented surfaces. Currently, this algorithm does not preserve the isotropic spectrum of the exiting angular flux upon reflection. If we instead use a *white* boundary condition our scheme captures the analytic solution exactly to the accuracy specified by our convergence criteria. But, to improve the existing reflecting boundary algorithm so that the exiting angular flux spectra is preserved would be an area for future work.

This problem is not a stressful test of a spatial discretization scheme, for the correct solution is simply constant. However, it does demonstrate the ability of UCB to operate on an unstructured hexahedral/tetrahedral mixed mesh, and also our implementation of reflective boundary conditions on arbitrarily oriented faces.

4 Summary and conclusions

We have successfully devised a wedge-based upstream corner-balance (UCB) method for three-dimensional grids of arbitrary polyhedra. The method has many desirable qualities. It satisfies robust and accurate equations in the thick diffusion limit, capturing linear solutions regardless of the grid. It has strict particle conservation and can use fully upstream transport sweeps, with no matrix inversions. It is algebraically linear yet stays non-negative in a source-free pure absorber.

Our wedge-based UCB scheme is not without drawbacks. Given a thick diffusive problem with a boundary layer that is not resolved by the grid, this method, with its "Marshak" boundary condition, runs the risk of being in error by up to a factor of two in the worst case. The method appears to be only 1st-order accurate; we do not believe it is possible to make it higher order as long as the only information transferred at wedge surfaces is the surface average.

One solution to these drawbacks could be to extend the *corner-based* UCB method to three-dimensional grids of arbitrary polyhedra. This is difficult because each corner can have a different shape and even a different number of faces. Nevertheless, such a corner-based method is worth pursuing for several reasons: it will likely be 2nd-order accurate or better; it should allow us to

build in a boundary condition that is much more accurate than Marshak; it should obtain the 1D UCB solution in a 3D problem that has 1D symmetry; and it should be less expensive than the wedge-based method because it will compute significantly fewer unknowns.

Acknowledgements

The authors would like to thank Jon Dahl, Jim Morel, Paul Nowak, Todd Palmer and Mike Zika for their comments and suggestions. Part of this work was supported by NSF grant No. CCR-9302782.

References

[Adams, 1998] M. L. Adams and P. F. Nowak, "Asymptotic Analysis of a Computational Method for Time- and Frequency-Dependent Radiative Transfer," *J. Comput. Physics*, **146**, 366-403 (1998).

[Adams, 1997] M. L. Adams, "Subcell Balance Methods for Radiative Transfer on Arbitrary Grids," *Transp. Theory Stat. Phys.*, **26**, Nos. 4&5, 385 (1997)

[McGhee, 1997] J. M. McGhee, R. M. Roberts and J. E. Morel, "Dante Boltzmann Transport Solver: An Unstructured Mesh, 3-D Spherical harmonics Algorithm/Compatible with Parallel Computer Architecture," LA-UR-97-1031, Los Alamos National Laboratory (1997).

[McGhee, 1996] J. M. McGhee and J. E. Morel, "NIKE/ATHENA Arbitrary Finite Element Upgrade," LA-UR-96-2124, Los Alamos National Laboratory (1996).

[Miller, 1998] R. L. Miller, "Development of a Discrete Ordinates Code System for Unstructured Meshes of Tetrahedral Cells, with Serial and Parallel Implementations," Ph.D. dissertation (Advisor: K. Mathews, Thesis Number AFIT/DS/DNP/98-02), Air Force Institute of Technology (1998).

[Morel, 1996] J. E. Morel, J. M. McGhee and E. W. Larsen, "A Three-Dimensional Time-Dependent Unstructured Tetrahedral-Mesh SPN Method," *Nucl. Sci. Eng.*, **123**, 319 (1996).

[Palmer, 1995] T. S. Palmer, "A Point-Centered Diffusion Differencing for Unstructured Meshes in 3-D," *Proc. Int. Conf. Mathematics and Computations, Reactor Physics, and Environmental Analyses*, Portland, Oregon, April 30 – May 4, 1995, Vol. 2. P. 897, American Nuclear Society (1995).

[Wareing, 1996] T. A. Wareing, J. M. McGhee and J. E. Morel, "ATILLA: A Three-Dimensional, Unstructured Tetrahedral Mesh Discrete Ordinates Transport Code," *Trans. Am. Nucl. Soc.*, **75**, 146 (Nov. 1996).